

Multi-Gbit/s LiFi Experiments with a VCSEL TX and an Enhanced Pulsed Modulation PHY

Malte Hinrichs, Giulio Boniello, Dominic Schulz, Ronald Freund, Volker Jungnickel

Abstract—Due to its better power efficiency, pulsed modulation such as on-off keying (OOK) has the potential of maximizing reach and minimizing energy consumption for future high data rate optical wireless communication (OWC), especially LiFi systems. In this paper, we introduce enhancements of the OOK-based Pulsed Modulation Physical Layer (PM-PHY) defined in IEEE Std. 802.15.13-2023. Namely, we evaluate robust line-coding and equalization techniques with reduced overhead and complexity, and increase bandwidth by using a vertical-cavity surface-emitting laser (VCSEL) array as transmitter. With these enhancements, we demonstrate data rates up to 4.25 Gbit/s using large VCSEL arrays with a combined optical power of 350 mW. These VCSEL arrays can cover an area of 4.32 m² at a distance of 2.5 m. Our results show that the large bandwidth, high power and low energy consumption of low-cost VCSEL arrays, when combined with pulsed modulation, can reach Multi-Gbit/s data rates and enable user mobility in large areas.

Index Terms—Optical wireless communication, Li-Fi, digital signal processing, power efficiency.

I. INTRODUCTION

Power limitations are one of the critical issues in optical wireless communication (OWC) systems. Most significantly, reach is limited by eye-safety regulations placing an upper bound on the transmitter power [1]. Thus, improved energy efficiency can be leveraged to increase the link reach and the coverage of OWC systems with user mobility, also denoted as LiFi, within the physical limitations. Another issue is the electrical energy usage in the transmitter circuitry, caused by amplification and biasing of the input waveform. Minimizing the corresponding heat dissipation in the optical frontend is a prerequisite for miniaturization. Furthermore, successful integration in mobile devices requires that battery lifetime is maximized.

In LiFi systems based on light-emitting diodes (LEDs), the available bandwidth is limited to 10s of MHz. To reach 1 Gbit/s, a waveform with high spectral efficiency is hence required. DC-biased optical OFDM (DCO-OFDM) is commonly used together with an adaptive bit- and power-loading

Manuscript received MMMM DD, YYYY; revised MMMM DD, YYYY;

... The research described in this paper was supported by the projects OWIND (Deutsche Forschungsgemeinschaft project No. 418775794), ELIOT (European Union's Horizon 2020 grant 825651), 5G-COMPASS (German Federal Ministry for Digital and Transport grant 19OI22017A). This work was based upon work from COST Action CA19111 (European Network on Future Generation Optical Wireless Communication Technologies, NEWFOCUS), supported by COST (European Cooperation in Science and Technology). The authors thank their partners in these projects for their valuable feedback.

The authors are with the Photonics Networks and Systems department at Fraunhofer Institute for Telecommunications, Heinrich-Hertz-Institut, HHI, Einsteinufer 37, 10587 Berlin, Germany (e-mail: malte.hinrichs@hhi.fraunhofer.de).

scheme with variable modulation formats on each sub-carrier, originally introduced in [2]. However, this approach requires drivers with high linearity, which is counterproductive for energy efficiency [3]. Moreover, the high peak-to-average power ratio (PAPR) of the DCO-OFDM waveform requires the control of clipping of negative signal components for intensity modulation and direct detection (IM/DD). In practice, this leads to a reduced modulation index, i.e., a lower percentage of the available optical power being modulated, which also reduces link reach and, with that, the service area in which communication with mobile devices is possible.

These limitations can be lifted by future use of laser-based transmitters for LiFi, e.g., based on arrays of vertical-cavity surface-emitting lasers (VCSELS), which enhance the available bandwidth into the GHz range [4]. With their massively increased bandwidth, laser-based transmitters will allow a paradigm change for LiFi: High data rates can now be realized with modulation schemes that have a lower spectral efficiency than orthogonal frequency-division multiplexing (OFDM), such as on-off keying (OOK). Because the PAPR of OOK is significantly lower than that of OFDM, a higher modulation index can be realized. Moreover, OOK relaxes the signal-to-noise ratio (SNR) requirements at the receiver. Both effects together improve reach and increase the size of the service area. Finally, OOK allows the use of switched-mode driver amplifiers, which avoid the operation of amplifier stages in a resistive mode and have the potential of reducing electrical energy usage by an order of magnitude compared to linear amplifiers [3], [5]. This advantage is also harnessed in fiber-based optical systems, where cost- and energy-efficient links tend to use high bandwidth OOK signals, as is also the case for some fiber-based Ethernet standards [6], [7].

A fundamental challenge in the design of OOK-based communication systems is the occurrence of baseline-wander, which is caused by high-pass characteristics of high-bandwidth analog frontends [8], [9]. This is traditionally addressed by the deployment of line codes [10], [11], which, however, have a trade-off between the degree of baseline-wander mitigation and overhead [12]. Linear equalizers can also effectively compensate baseline-wander [13], [14]. We have previously developed a physical layer (PHY) based on OOK modulation addressing this issue that is included in IEEE Std 802.15.13-2023, where it is denoted as Pulsed Modulation PHY (PM-PHY) [3], [15]. Link-level simulations and experiments have shown that this PM-PHY can deal with typical bandwidth limitations of LED-based LiFi frontends and in the optical wireless propagation channel, and achieve high robustness and long reach [3], [16]. Moreover, its design is similar to

the existing High Bandwidth PHY (HB-PHY) defined in the same standard for using OFDM modulation, which in turn is derived from ITU-T Recommendations G.9960 (G.hn) [17] and G.9991 (G.vlc) [18].

This similarity is an important feature, as the central idea of the PM-PHY is to enable the (re-)use of efficient real-time processing hardware developed for OFDM-based applications with minimal modifications. For this reason, the PM-PHY is designed around the application of frequency domain equalization (FDE) similar to OFDM systems, using a block structure with cyclic prefixes (CPs). This way, the advantages of OOK modulation for optical links can be realized using highly efficient hardware implementations of fast Fourier transform (FFT)-based signal processing that are now used for a wide range of communication systems, from cost- and energy-efficient Internet of Things (IoT) devices to high-bandwidth Wi-Fi and 5G networks that provide data rates in the Gbit/s range to battery-powered handheld devices [19], [20]. Nonetheless, we further consider and optimize line coding for the PM-PHY as a low-complexity option for systems that do not deploy equalization. Because the main design goal was robustness rather than high data rates, the PM-PHY relies on widely-used 8b10b line coding to overcome high-pass effects in DC-biased optical frontends (OFEs) commonly used for LiFi. This is a very effective solution, but adds an overhead of 25 %. The 8b10b code is also intertwined with Reed-Solomon (RS) forward error correction (FEC) in the PM-PHY, increasing complexity. A second source of overhead is the CP for the application of FDE, as only very short and very long CP options are defined (1/32 and 1/4 of the block length).

In the present work, we enhance the PM-PHY by extending its bandwidth, introducing new line coding options, and optimizing equalization, with the goal of minimizing the overhead while effectively compensating baseline-wander. The equalizer is additionally exploited to maximize the usable bandwidth of OFEs and multipath channels. For line-coding, two scrambler-based schemes are studied that have much lower overhead than 8b10b. For FDE, the impact of CP length on performance is analyzed in combination with these alternative line coding schemes, and more efficient CP settings are derived. As a lower bound on overhead, time domain equalization (TDE) is also investigated.

The objective of this work is to explore a high-bandwidth LiFi transmitter based on VCSEL arrays with OOK modulation, using the enhanced PM-PHY, to enable multi-Gbit/s LiFi transmission with long reach, low energy consumption, and minimal overhead. While the use of VCSEL arrays massively enhances the bandwidth of the optical source, high-power laser drivers and optical receivers have bandwidth limitations that warrant the use of effective equalization to enhance the usable system bandwidth also in this case. The main contributions of this work are to i) add a complete look at the state of the art, ii) summarize preliminary results previously reported in [21]–[23], iii) describe a new channel interpolation technique which improves the frequency-domain equalizer performance, and iv) present new experimental results using a fiber-coupled high-bandwidth receiver to assess the bandwidth

limitation in our VCSEL based LiFi transmitter.

This article is structured as follows: Sec. II gives an overview of the state of the art of pulsed modulation and laser-based transmitters in OWC, Sec. III introduces the line-codes and equalizers under consideration, Sec. IV presents the setups used for simulations and experiments, Sec. V presents the corresponding results, and finally a conclusion is drawn in Sec. VI.

II. STATE OF THE ART

This section presents the state of the art around pulsed modulation based OWC and laser-based OWC transmitters.

A. Pulsed Modulation for Optical Wireless Communication

Using OOK instead of OFDM with higher order modulation effectively trades spectral efficiency for bandwidth, allowing a reduced transmitter power for a given data rate [24], [25]. For this approach, sufficient analog bandwidth is required. In fiber-optical communication this is often the case when operating at 10 Gbit/s, e.g., using standards such as 10 Gigabit Ethernet and XG-PON that are based on non-return-to-zero (NRZ)-OOK [7], [26]. Similarly, OOK has been used to maximize optical power utilization and reach in early works on OWC, such as in the IrDA standard [27], and in research on diffuse optical wireless links [1]. When using high-power LEDs for OWC with a range of several meters, however, bandwidth is limited to 10s of MHz. To reach data rates of 1 Gbit/s, DCO-OFDM with adaptive bit-loading was introduced which maximizes spectral efficiency [2], [28], [29]. Extending the data rate beyond this mark is becoming possible with laser-based LiFi frontends [30], of which the development is discussed in the following section.

The main energy saving effect for OOK modulation in OWC is due to the limitation to only two modulation states. First, this means that the driver design can be much simplified, because only on and off switching is required instead of digital-to-analog converters (DACs) and linear amplification. This enables substantial electrical energy savings with accordingly designed transmitters [3], [5]. Second, OOK has a very low PAPR. Considering a signal representation with fully on and off states, the PAPR of OOK is 2 for equiprobable marks. In a balanced representation of the electrical signal (e.g., symbols represented by ± 1), the PAPR is equal to 1 for an ideal rectangular pulse shape. For OWC, the PAPR is particularly important to maximize the reach of the link. Due to the decay of optical power being proportional to the square of the distance in the non-directed optical channel, and the square relationship between optical and electrical power, the electrical SNR varies with the fourth power of the transmission distance [1]. This means that under limited peak power, a modulation format with a PAPR of 10, as common for OFDM [31], theoretically reaches a given electrical SNR at a distance $(\sqrt[4]{10})^{-1} \approx 0.56$ times that of OOK.

Several analytical and simulative evaluations of OOK and pulse amplitude modulation (PAM), of which OOK is a special case, have been carried out in comparison with multi-carrier formats, using a range of different system parameters and

equalization techniques [32]–[37]. A universal conclusion is difficult to draw, but an advantage in energy efficiency is generally found for pulsed modulation due to the lower PAPR of its waveforms and the required biasing or clipping of OFDM in optical use cases. Furthermore, higher order PAM is found to reach comparable spectral efficiency and computational complexity when combined with suitable equalizers. We have previously conducted an experimental evaluation of OOK and OFDM using linear frontends, where we showed a significantly larger reach for OOK [25]. However, conclusive results comparing a modern OFDM implementation using adaptive bitloading to the enhanced PM-PHY in combination with an optimized OOK transmitter have not yet been presented. In this work, we aim for optimizing OOK transmission for OWC in the context of FFT-based signal processing, to enable a fair comparison with mature OFDM-based standards in the future.

To mitigate the baseline wander effect caused by high-pass filtering of OOK and multi-level pulse amplitude modulation (M-PAM) signals in analog frontends, line coding is commonly used, which suppresses low frequency components in the modulated signals. A simple solution is Manchester coding [38], [39]. It doubles the required bandwidth, but is very effective and has low complexity. The OOK-based PM-PHY defined in the standard IEEE 802.15.13-2023 [15] uses 8b10b line coding [10] and combines it with FDE. This approach has originally been evaluated in the context of multi-level PAM in conjunction with 5b6b line coding, which is also part of 8b10b [13], [14]. In these works, it was found that the combination of line-coding and equalization can overcome the baseline wander effect up to an effective high-pass cut-off frequency of $f_c \approx 0.025R_b$, relative to the symbol rate R_b . For using zero-forcing (ZF)-FDE with M-PAM in OWC, it was shown that in order to maximize power output, it is beneficial to utilize the full available bandwidth with 2-PAM (i.e., OOK) at a high symbol rate, and only move towards higher modulation orders for the highest data rates in good channel conditions [40]. In this work, we focus on OOK, with higher order PAM remaining an option for future enhancements.

For linear equalization, TDE can be used, but for channel impulse responses (CIRs) longer than 5 symbol periods, the computational effort is higher than that of FDE [41]. In our case, this condition is fulfilled for the band-limited LED frontends at high symbol rates. A further motivation for using FDE in the context of the standard IEEE 802.15.13-2023 is compatibility with algorithms used in OFDM, as described in Sec. I, to benefit from existing real-time signal processing hardware. Frequency domain pre-equalization for OOK was also shown to effectively enhance the usable bandwidth and prevent noise-amplification [42]. For pre-equalization, multi-level DACs and channel knowledge are required at the transmitter, though, which complicates system design and negates one of the main benefits of using OOK, which is the simple and efficient transmitter design.

Non-linear equalizers can counter distortions arising from driving optical sources outside of their linear range. Solutions that have been analyzed in this context are decision feedback equalization (DFE) [1], [43], [44] and Volterra equalization [45], [46], also in conjunction [47], for post-, and Tomlinson-

Harashima precoding (THP) for pre-equalization [48]. Volterra equalization was found to be well suited for characterizing and compensating non-linear distortions caused by LEDs, without prior knowledge of specific device parameters [45]. However, especially when aiming for long reach, receiver noise tends to be the main limitation in OWC links, and optimizing the transmission power or deploying an automatic gain control (AGC) at the receiver has a larger benefit than non-linear equalization [49], [50].

The computational complexity of the discrete Fourier transform (DFT) and inverse discrete Fourier transform (IDFT) operations for PAM-FDE is identical to that of DCO-OFDM for a given symbol rate and DFT length. However, as PAM signals are defined in time domain, the conversion to frequency domain is only carried out at the receiver before channel estimation and equalization, and not at the transmitter as for OFDM. This shift of the IDFT operation does not affect the overall complexity of the system, but could be exploited in hybrid systems that use OFDM in the downlink and single-carrier (SC)-FDE or PAM-FDE in the uplink: In this case, the IDFT moves from the transmitter side in the mobile terminal into the receiver, which is located at the base station. This halves the computational complexity for (I)DFT at the mobile terminal, since only the DFT for the demodulation of OFDM signals in the downlink remains [41].

As indicated previously, for our considerations, we focus on linear FDE. Its complexity does not depend on the length of the CIR, and as stated above, it is widely used in mass-market solutions for mobile communication already. The main drawback of this solution is the overhead caused by CPs, which indeed depends on the expected length of CIRs. In the evaluations of the VCSEL-based transmitter, linear TDE is additionally included in the evaluations to analyze its throughput independent of CPs.

B. Laser-based Optical Wireless Frontends

As discussed above, current OWC technology is limited by the modulation bandwidth of high-power LEDs, which produce light based on spontaneous emission. With sophisticated LED driver designs, up to 100 MHz 3 dB-bandwidth have been reached [49], which is comparable to 5G and recent 802.11 ac/ax Wi-Fi systems in the radio frequency (RF) domain. With laser diodes, due to stimulated light emission, the modulation bandwidth can be extended into the GHz range, so that a significant increase in data rate is attainable [1], [51].

In fiber-optical systems, low-cost VCSELs have been demonstrated to offer modulation bandwidths and data rates reaching tens of GHz and more than 200 Gbit/s, respectively, using modulation schemes with high spectral efficiency such as PAM and discrete multi-tone (DMT), which is similar to OFDM [52], [53]. These results show the high potential of VCSELs as new light sources also for OWC. In first VCSEL-based OWC trials, the optical emitters were coupled with commercial power line communication terminals [54], covering a distance below 40 cm. The transmission of 2.125 Gbit/s OOK signals over a distance of 2.8 m was demonstrated in a static setup [55], but using a lens at the transmitter focusing the

optical power onto the receiver. In a similar scenario, mobility of the receiving terminal was studied [56], demonstrating a covered area of 0.01 m^2 at 3 m distance at a data rate of 1.25 Gbit/s.

Data rates well in the tens and hundreds of Gbit/s range have been demonstrated for OWC with various types of lasers, either forming narrow beams focused on the receiver [57], [58], or using short link distances up to 1 m [59], [60], but the coverage of larger areas for OWC is in these cases not implemented, as the modulated optical power is too low. The transmission of 26 Gbit/s was demonstrated across a distance of 2 m using subcarrier modulation across three wavelengths [61]. Wide-area coverage at high data rates has been realized by forming a narrow beam and steering it towards the receiver [62]–[64]. These systems tend to have a high complexity and large form factors, though, which makes future system integration difficult. Furthermore, protocol overhead occurs for adaptive beam-search, as known from mm-wave standards such as IEEE 802.11ad and 802.11ay [65], [66]. A coverage of 2.27 m^2 at a distance of 1.85 m with a data rate of 2.55 Gbit/s has been reached using OFDM with a 200 mW Fabry-Pérot laser-diode and a custom diffusor [67].

Single VCSELs provide low optical power in the order of few milliwatts and, thus, do not allow transmission with a large coverage area in which the user can move freely. This is also an issue for light detection and ranging (LIDAR) applications, where as a solution between 10s and 1000s of VCSEL apertures are arranged in 2D arrays on the same semiconductor chip to reach high optical power [68]. Combined with diffusors, laser emitters in the required power range can be used in eye-safe LiFi transmitters similar to high-power LEDs [67]. This allows us to exploit the enhanced bandwidth of VCSELs at the optical power levels needed to keep the range and coverage comparable to recent LED-based OWC systems. This way, a new generation of LiFi systems becomes possible that can reach data rates in the order of 10 Gbit/s per OWC link, with overlapping cells for seamless mobility support similar to current radio-based systems [69].

Accordingly, in this work we follow the classical approach in mobile communications, i.e., provide enough power to cover a large area and increase the bandwidth to enhance the data rate. We demonstrate that high transmitter power can be reached by means of VCSEL arrays and limiting amplifier drivers, which enable OOK at high symbol rates. Our transmitter uses no lens and provides a wide beam covering an area suitable for practical LiFi deployment. The emission cone is shaped by a diffusor directly attached to the VCSEL arrays, which also ensures eye-safety. We use post- instead of pre-equalization to keep the transmitter simple and drive the modulation bandwidth as high as possible, as described above.

III. DIGITAL SIGNAL PROCESSING FOR HIGH-BANDWIDTH OOK OWC

The following subsections describe new digital signal processing (DSP) techniques evaluated in this work with the goal of enhancing the performance for practical OOK-based OWC.

The focus is on line coding and equalization, which requires precise channel estimation. In both cases, different solutions that address signal distortions caused by band pass limitations in the analogue OFEs are analyzed, looking for an optimal trade-off between overhead and effectiveness. For comparison of the techniques, the effective payload data rate R_{data} is calculated from the symbol rate R_{sym} according to:

$$R_{\text{data}} = \frac{R_{\text{sym}}}{r_{\text{code}} r_{\text{CP}}} \quad (1)$$

with r_{code} denoting the relative overhead of line coding and r_{CP} the relative overhead caused by CP insertion, with the overhead in percent given by $(r_{\text{code/CP}} - 1) \cdot 100\%$, and $r_{\text{code/CP}} = 1$ corresponding to the case with no overhead caused by the respective factor. As this equation considers only the data rate achieved for payload transmission with the given coding schemes, the channel estimation sequence and other protocol overhead is not considered.

A. Efficient Line Coding

Three algorithms for DC removal on the input data stream are compared in this work. As a baseline, the line code 8b10b is described, which is the original solution for the PM-PHY in IEEE Std 802.15.13-2023. Next, a guided scrambler with a 64b67b configuration and the scrambler used in the 64b66b line code are presented. These codes were selected with the goal of finding the optimal balance between line-coding overhead and the grade and determinism of the removal of low-frequency signal components and baseline wander [70].

1) *8b10b Line Code*: The 8b10b line code [10] is codebook-based and replaces 8-bit bytes with 10-bit code words, resulting in a DC-free data stream with a maximal run length of 5. The code uses a limited alphabet of valid code words with well-defined properties. For each possible byte, the encoder selects a code word based on the cumulative disparity after encoding of the previous word, so that the maximum variation of the cumulative digital sum is bounded to 6. While the properties of this code are very favorable for transmission across AC-coupled circuits, an overhead of 25% is generated ($r_{\text{code,8b10b}} = 5/4$), as two additional bits are inserted for every byte.

2) *64b67b Guided Scrambler*: The 64b67b line code describes a specific implementation of a guided scrambler [11]. This technique builds on a self-synchronous scrambler that is used to generate a set of code words for any given sequence of input data by prepending different sequences of augmentation bits and scrambling each so extended sequence. The optimal code word can then be selected out of the resulting set based on metrics such as run lengths, running disparity, frequency of symbol transitions, or similar. This selection shapes the statistical distribution of the output code words, e.g., by favoring words with shorter run lengths. The number of augmentation bits determines the amount of code words to select from as well as the resulting overhead. We consider a code that builds on a linear-feedback shift register (LFSR) with the polynomial $G(x) = x^{n_a} + 1$ and $n_a = 3$ augmentation bits, based on the proposition for balanced transmission with

high transition density in [11]. This results in an overhead factor of $r_{\text{code},64b67b} = 67/64$, or an overhead of 4.7 %, for an input word length of 64 bits. The code word is selected by using the following criteria in order: highest number of symbol transitions, lowest running disparity at the end of the word, lowest maximum run length, random selection. Note that the scrambler used here is not related to the scheme defined in the Interlaken protocol, also named 64b67b [71].

3) *64b66b Scrambler*: The 64b66b line code was developed for the 10 Gbit/s Standard IEEE Std 802.3ae [7]. 64b66b does not use fixed code words, but only a self-synchronous scrambler to randomize the input data. Scrambler and de-scrambler are based on LFSRs implementing the polynomial $G(x) = x^{58} + x^{39} + 1$. The scrambler does not add any overhead, but the 64b66b code defines two bits for control information at the beginning of each 64-bit sequence, effectively forming 66-bit code words and creating an overhead of 3.1 %. Since these control bits do not influence the operation of the scrambler in any way, though, and are not required for the operation of the PM-PHY, we omit them and focus solely on the scrambler for our evaluation. Hence, no overhead is added ($r_{\text{code},64b66b} = 1$). In contrast to 8b10b, run lengths and running disparity are bounded statistically, resulting in the properties of its output being very similar to uncoded random data. For this reason, random data is used as a reference in case of the LED-based experiments instead of this scrambler.

Note that the nesting of RS-based FEC and line coding defined in the PM-PHY is maintained also for the scrambler-based approaches used here. FEC decoding is not carried out, however.

B. Channel Estimation and Equalization

This section describes channel estimation (CE) and equalization techniques used in this work. First, the sequence used as a reference for CE at the receiver is described, followed by the methods used for FDE and TDE.

1) *Channel Estimation Sequence*: As a basis for channel estimation, we used the channel estimation sequences defined in the PM-PHY. They consist of m-sequences (*maximum length* or *maximal* sequences) [72] of different lengths N_m . They have well-defined auto-correlation properties and, due to their pseudo-random characteristics, signal power is distributed relatively evenly in the frequency domain, which is important for channel estimation. As $N_m = 2^n - 1$, with n the length of the generating LFSR, a single symbol with the value -1 is appended to each sequence to match the PM-PHY block lengths $N_B \in \{64, 128, 256, 512, 1024\}$ symbols for the respective symbol rates $R_{\text{sym}} \in \{12.5, 25, 50, 100, 200\}$ MBd and to balance the number of positive and negative symbols per sequence. For the measurements with variable symbol rate using the VCSEL transmitter, $N_B = 1024$ symbols is always used.

2) *Frequency Domain Equalization Using Binary Channel Estimation Sequence*: To facilitate FDE, the received signals are transformed to the frequency domain using the FFT, and equalization is then carried out block-wise by division with the estimated channel frequency response:

$$\hat{X}(f) = \frac{Y(f)}{\hat{H}_B(f)} \quad (2)$$

where Y is the block-wise frequency domain representation of the received signal, \hat{H}_B that of the estimated channel response after interpolation (described below), and \hat{X} the equalized received signal. \hat{X} , Y , and \hat{H}_B are vectors of length N_B . For application of the FFT, pseudo-cyclic blocks of length N_B are formed in the transmitted signal by inserting CPs of length N_{CP} into the time domain signal, resulting in an overhead factor of $r_{\text{CP,FDE}} = 1 + N_{\text{CP}}/N_B$.

Despite the signal power of the estimation sequence being largely evenly distributed over the frequency range, on the small scale, the distribution is noise-like and the power of individual frequency bins underlies large fluctuations. This is due to the pseudo-random nature of the binary Gold sequence, and is clearly visible in its base-band spectrum shown in Fig. 1a. For frequency domain channel estimation, this is detrimental: Every frequency bin is estimated independently, and the quality of the estimation varies significantly with the power in the reference signal for that bin, as low power in the reference leads to noise enhancement.

To overcome this, we propose a linear minimum mean square error (LMMSE) interpolation approach first investigated for OFDM [73] to smooth the estimated channel response:

$$\hat{H}_B = \mathbf{W}^{lmmse} \cdot \tilde{H}_P \quad (3)$$

where \mathbf{W}^{lmmse} is the $N_B \times N_P$ LMMSE interpolation matrix, and \tilde{H}_P the non-interpolated channel response estimated with the least squares (LS) method on all pilot frequencies, a vector of length N_P . Here, \tilde{H}_P contains all frequency bins where the spectrum of the estimation sequence has a power above the threshold P_{thr} , as shown by the dashed line in Fig. 1a. P_{thr} is set to $P_{\text{thr}} = 0.35P_{\text{avg}}$ for LED transmissions, with P_{avg} the average power of the estimation sequence, and $P_{\text{thr}} = 0$ for the high bandwidth VCSEL transmissions. Both values were empirically found by optimizing for error vector magnitude (EVM) after equalization using experimental data. The gaps in the spectrum created by the application of the power threshold are bridged by the interpolation.

\mathbf{W}^{lmmse} is calculated as follows, depending on the SNR and the time constant τ_d of an assumed exponentially decaying power delay profile (PDP) of the channel response as recommended in [73]. Instead of splitting the frequency band into chunks as in that work, we interpolate across the whole band in a single step. Accordingly, matrices and vectors related to chunks, originally denominated with the index C, are referring to blocks here and are denominated with the index B:

$$\mathbf{W}_{\tau_d, \text{snr}}^{lmmse} = \mathbf{F}_{BL} \bar{\mathbf{R}}_{h_L h_L} \mathbf{F}_{PL}^* (\mathbf{F}_{PL} \bar{\mathbf{R}}_{h_L h_L} \mathbf{F}_{PL}^* + \frac{1}{\text{snr}} \mathbf{I})^{-1} \quad (4)$$

where \mathbf{F}_{BL} the $N_B \times N_L$ block DFT-matrix, \mathbf{F}_{PL} the $N_P \times N_L$ pilot DFT-matrix, and \mathbf{F}_{PL}^* its complex conjugate. $\mathbf{R}_{h_L h_L} = \text{diag}(\sigma_0^2 \dots \sigma_{N_L-1}^2)$ is the autocorrelation matrix of the channel, a diagonal matrix that represents its PDP, i.e., the power in

each tap of the CIR. The PDP is described by the exponential decay $\sigma_l^2 \sim e^{-\frac{l}{\tau_d}}$, $l \in \{0 \dots N_L - 1\}$ defined by τ_d . $\bar{\mathbf{R}}_{h_L h_L} = \frac{\mathbf{R}_{h_L h_L}}{\text{trace}(\mathbf{R}_{h_L h_L})}$ is the normalized PDP. N_L is the length of the channel response, which is assumed equal to N_{CP} , and N_P the number of pilots. Unless stated otherwise, all results presented in this work are based on channel estimates interpolated with $\mathbf{W}_{\tau_d, snr}^{lmmse}$ with the assumptions $\tau_d = N_{CP}/2$ and $snr = \widehat{snr}$, which is the estimated SNR obtained by singular value decomposition (SVD) as suggested in [73].

Compared to [73], the pilot distribution is significantly different: The majority of frequency bins is used for channel estimation here, so the “pilots” are densely packed across the band instead of sparsely distributed. This is because only those bins with powers under the power threshold P_{avg} are excluded from the estimation, making much more base points available for the interpolation. The large number of pilots causes the calculation of the interpolation matrix to be computationally relatively expensive, though. However, the channel includes frontend effects and propagation. While OFE effects may be frequency-selective and static, the LOS-based propagation channel is frequency-flat but varies over time, due to mobility. To reduce complexity, the equalizer can be built from two contributions: a static part to compensate the OFE and a simpler dynamic part adapting to wireless propagation.

As a potential alternative, we evaluated a simplified version of the interpolation matrix $\mathbf{W}_{\tau_d, snr}^{lmmse}$ based on the idealized assumptions $\tau_d = \infty, snr = \infty$, as shown in the following [73]. First, setting $\tau_d = \infty$ yields a $\bar{\mathbf{R}}_{h_L h_L}$ with all diagonal elements equal to $1/N_L$, simplifying (4) to:

$$\mathbf{W}_{\infty, snr}^{lmmse} = \mathbf{F}_{BL} \mathbf{F}_{PL}^* (\mathbf{F}_{PL} \mathbf{F}_{PL}^* + \frac{N_L}{snr} \mathbf{I})^{-1} \quad (5)$$

Also setting $snr = \infty$ causes the right term of the inverted part to disappear completely, leading to a further simplification:

$$\mathbf{W}_{\infty, \infty}^{lmmse} = \mathbf{F}_{BL} \mathbf{F}_{PL}^+ \quad (6)$$

The generation of the resulting interpolation matrix $\mathbf{W}_{\infty, \infty}^{lmmse}$ requires only the calculation of the Moore-Penrose pseudo-inverse of the pilot DFT-matrix \mathbf{F}_{PL}^+ and a multiplication with \mathbf{F}_{BL} , and, more importantly, is not dependent on any channel parameters, which reduces complexity at runtime. Since most of the frequencies in the spectrum are used for channel estimation, \mathbf{F}_{PL} is similar to the full DFT-matrix.

The effects of the two approaches for interpolation are visualized by Fig. 1b. It shows the impact of the interpolation matrices $\mathbf{W}_{N_{CP}/2, \widehat{snr}}^{lmmse}$ and $\mathbf{W}_{\infty, \infty}^{lmmse}$ on the spectrum of an exemplary channel response recorded at 1 GBd using the VCSEL-based transmitter and a Thorlabs APD210 receiver. The power threshold is set to $P_{thr} = 0$, so that all frequency bins except $f = 0$ are used for the initial estimate before the interpolation. The graph without interpolation shows a generally noisy characteristic, and large peaks protruding from the estimated response both towards higher and lower powers. The interpolated graphs both clearly show the smoothing effect of the interpolation. The noise amplification peaks are virtually non-existent any more. The different assumptions about PDP

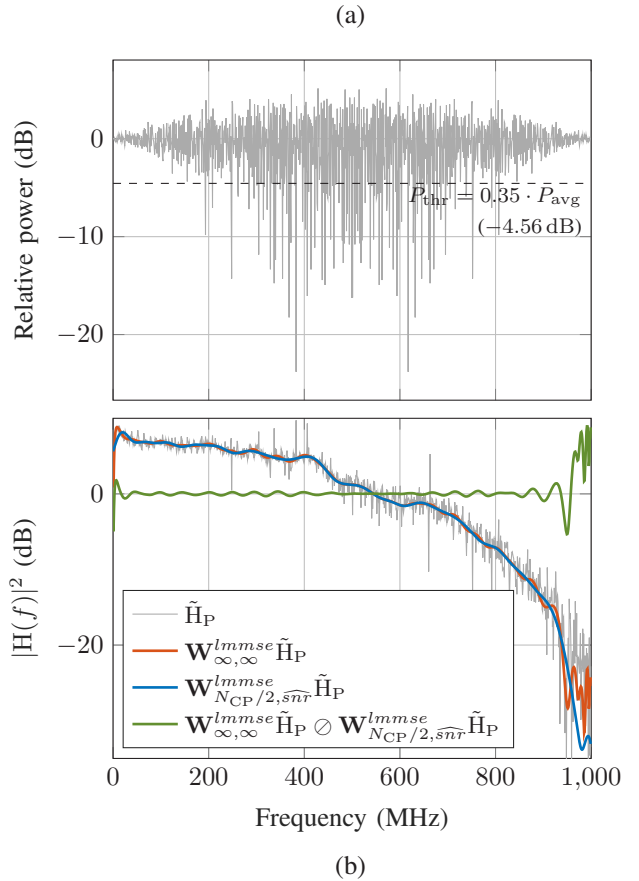


Fig. 1. (a) Spectrum of the channel estimation sequence, a balanced Gold sequence of length 1024. The value of $P_{thr} = 0.35P_{avg}$, used for the LED-based setup, is shown for reference. (b) Magnitude of an LS estimate of the channel response with and without interpolation. Notably, the positions of noise peaks standing out of the non-interpolated estimated channel response correspond with low power frequency bins in the spectrum of the estimation sequence. The ratio of the two interpolated responses, calculated by the Hadamard or element-wise division denoted by the operator \oslash , is shown for reference.

and SNR mostly have an effect on the small scale in this example. With the SNR estimation and $\tau_d = N_{CP}/2$, a stronger averaging effect seems to be present, but the deviations between the two interpolated responses are minor overall. The ratio between the two interpolated responses shows larger deviations only at the edges of the spectrum, not exceeding ± 0.5 dB in the center range that covers 86.4 % of the observed spectrum. The impact of simplifying the interpolation on error levels of the equalized signals is evaluated in Sec. V-A.

3) Channel Estimation for Time Domain Equalization: For time domain equalization, a 10-tap finite impulse response (FIR) filter was used at symbol rate. The filter coefficients were estimated using the LS method based on the m-sequence inserted for channel estimation. TDE is applied to the continuous signal and the CP is not required and can be omitted to reduce overhead ($r_{CP, TDE} = 1$). In our measurements, the CPs were still part of the transmitted signals, but were disregarded for the further signal processing and data rate calculations with the TDE. This equalizer was only evaluated for the VCSEL based measurements.

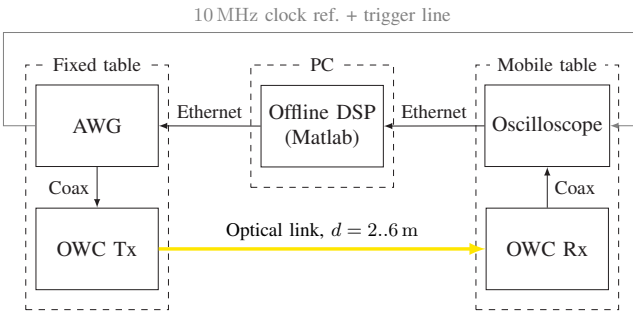


Fig. 2. Experimental setup for LED-based evaluations.

IV. EVALUATION FRAMEWORK

In the following, the framework for evaluation of the line coding techniques is presented. First, the experimental setup with LED-based OFE prototypes is given. Our goal was to assess if the 8b10b line coding can be replaced by a more efficient option, with and without equalization. Additionally, we looked into optimizing the length of the CP for a further reduction of the overhead.

In a second step, laser (VCSEL) based setups were evaluated, in order to assess the achievable coverage and data rate. To that aim, we applied the findings from the LED-based setup and, moving away from the current PM-PHY definition, added TDE to the evaluation, which allows omitting the CP.

As mentioned in Sec. III-A, the line coding techniques were deployed without transmission of any control information. This means that only the scrambler was applied for 64b66b, and no overhead was created by this algorithm. Nevertheless, the scramblers are referenced by the name of the codes they are used in, i.e., 64b66b and 64b67b.

A. LED-based Experimental Setup

To assess if the overhead of the 8b10b line coding can be reduced, an experimental setup based on LED-based OFE prototypes was used, which is shown by the block diagram in Fig. 2. A second aspect regarded for overhead optimization in this setup was the length of the CP, which is required for FDE. The impact of the LMMSE channel interpolation on the results of FDE was also studied. The setup comprised two OFEs, of which one was connected to a Tektronix AWG5012 arbitrary waveform generator (AWG) on the transmitter side and the other to a Teledyne LeCroy WavePro 804HD oscilloscope operating at a sample rate of 1 GS/s on the receiver side. Signal processing was carried out offline in Matlab. The distance between the transmitter and receiver was varied between 2 and 6 m in steps of 0.5 m. AWG and oscilloscope were connected via direct lines for clock synchronization and triggering. The combined frequency response of the transmitter and receiver frontends used here is similar to that measured and approximated in [70] by a series of infinite impulse response (IIR) high- and low-pass filters with -3 dB cut-off frequencies up to 200 kHz for the high- and down to 20 MHz for the low-pass sections. A vector network analyzer (VNA) measurement of a line-of-sight (LOS) transmission across 1 m distance was used as a reference in that work. An

attenuation of -10 dB was reached around 60 MHz, -20 dB around 110 MHz.

The transmitted signals contained a series of PM-PHY frames (PHY protocol data units, PPUDUs) consisting of preamble, header, payload, and channel estimation sections [15]. Only the payload channel estimation sequence and the payload itself were processed, and the synchronization sequence was used for frame synchronization. All symbol rates defined for the PM-PHY $R_{\text{sym}} \in \{12.5, 25, 50, 100, 200\}\text{MBd}$ were evaluated. 1,048,576 bits of random data were transmitted for each measurement, distributed across 64 frames and split into blocks of $N_B = R_{\text{sym}}T_B$, with $T_B = 5120\text{ ns}$. CP length N_{CP} was varied between the short ($\frac{1}{32}N_B$) and long ($\frac{1}{4}N_B$) settings defined for the PM-PHY, with additional medium settings of $\frac{1}{8}N_B$ and $\frac{5}{32}N_B$. The performance of payload data coded with the 64b67b and 8b10b line codes was compared to uncoded random data. The channel was estimated in frequency domain based on the transmitted estimation sequences, and FDE was applied. The power threshold of the interpolation algorithm described in Sec. III-B2 was set to $P_{\text{thr}} = 0.35P_{\text{avg}}$.

We observed initially that the equalizer performance was slightly degraded, especially at high symbol rates, due to small synchronization offsets on the sub-symbol scale, causing a “bleeding in” from the CP of the following block. This effect was overcome by applying a time delay of 4 % of the respective CP length to the signal before CP removal at the receiver, effectively shortening the CP. The small delay creates a cyclic shift within the block and CP which translates to a phase shift in the frequency domain, being fully compensated by the channel estimation and equalizer. For demodulation without equalizer, such delay was not applied.

B. VCSEL-based Experimental Setup

For operation at symbol rates of 1 GBd and above, the PM-PHY and its enhancements introduced above were evaluated using a transmitter prototype, shown in Fig. 3a, that combines commercial VCSEL arrays with diffusors and several integrated limiting amplifier drivers developed for small form-factor pluggable (SFP) modules, i.e., energy efficient optical fiber communication. Our prototype carries four drivers of the type Maxim MAX3736 and four VCSEL arrays of the type Brightlaser VD-0940V-140M-1C-5A1. The drivers have a maximum specified symbol rate of 3.2 GBd and AC modulation current of 85 mA. These components were selected based on market availability, with the goal of reaching a bandwidth greater than 1 GHz while approaching an output power of 1 W.

Sets of two drivers in parallel drive series of two VCSEL arrays each, doubling the effective drive current at the lasers. The drivers are connected in AC mode and the modulation current is added to a bias of $\approx 50\text{ mA}$. Each VCSEL array features 10 apertures and is specified for an optical output power of 140 mW at a forward current of 89 mA with a wavelength of 940 nm. The diffusors mounted on the VCSEL arrays have emission angles of 60° in the x- and 45° in the y-direction. We measured a combined average optical output power of 350 mW for our prototype using a Thorlabs PM300 optical power meter.

Eye safety is maintained for our transmitter due to the used diffusors. They increase both the effective emitter area and the emission angle of the VCSEL arrays, making the power distribution similar to that of high-power LED transmitters. For classification as a Class 1 source according to IEC 60825-1, the maximum permissible exposure (MPE) for an exposure time of 3×10^4 s is relevant, measured at a distance of 10 cm from the source. In that setup, our VCSEL arrays have an apparent size of 25 mrad, and are emitting at a wavelength of 940 nm [74]. With these parameters, the calculated MPE is 509.4 W/m² for the cornea and 100 W/m² for the skin for large area exposal [75]. With the specified optical power of 140 mW and the emission angles of the attached diffusors of 60° and 45° in the x- and y-direction, respectively, an exposure of 14.6 W/m² results, fulfilling the eye and skin safety requirements.

In order to demonstrate the suitability of VCSELs for LiFi in the Gbit/s range, we evaluated the prototype in three setups with different receivers and for various transmission distances: a first one focusing on the achievable coverage, a second one on evaluating the line codes and equalizers for a higher range of symbol rates, and a third one looking at the maximum achievable throughput of the transmitter. In all setups, the transmitter was connected to a Keysight M8190A AWG, and the respective receiver to a Teledyne LeCroy WavePro 804HD oscilloscope running at 20 GS/s. Digital signal processing was carried out offline in MATLAB in all cases.

The transmitted OOK-signals consisted of the PM-PHY channel estimation sequence of length $N_B = 1024$ symbols, which in this case was fixed for all symbol rates, and line-coded random data divided into blocks of the same length and enhanced with CPs of length $N_{CP} = \frac{1}{8}N_B = 128$ symbols.

1) Coverage Measurement Setup: For the evaluation of the achievable coverage, a commercial Thorlabs APD210 receiver with a 3 dB pass-band from 5 to 1000 MHz was used, shown in Fig. 3b. To focus more optical power on the receiver, the receiver was combined with a lens with a diameter of 25.4 mm and a focal length of 34.9 mm located at a distance of 30 mm from the avalanche photodiode (APD). This was required due to the small size of the high-bandwidth photodetector, and made accurate alignment of the receiver necessary. While this is unpractical for mobile communication systems, solutions such as imaging photodiode-arrays with both the required bandwidth and large field-of-view are subject of ongoing research [76]–[78]. The receiver was placed at distances of 1, 1.75, and 2.5 m from the transmitter (Tx), denoted as z-distance, and then moved at distances between 0 and 1.2 m away from the z-axis, denoted x-offset. At every position, the receiver was rotated so that the lens was aligned with the transmitter and the optical power was focused onto the photodiode, as shown by the schematic of the setup in Fig. 4.

For the coverage measurement, 8b10b line coding was applied and FDE was used at the receiver, with LMMSE interpolation of the channel response and $P_{thr} = 0$ (Sec. III-B2). Per measurement, 65,536 data bits were transmitted in the payload. The symbol rate was varied between 1 and 2.5 GBd in steps of 500 MBd.

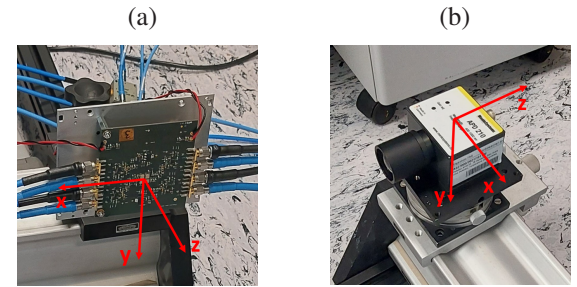


Fig. 3. Photos of the coverage measurement setup. (a) Transmitter prototype with four VCSEL arrays behind diffusors. (b) Commercial receiver (Thorlabs APD210) with 35 mm lens (diameter 25.4 mm).

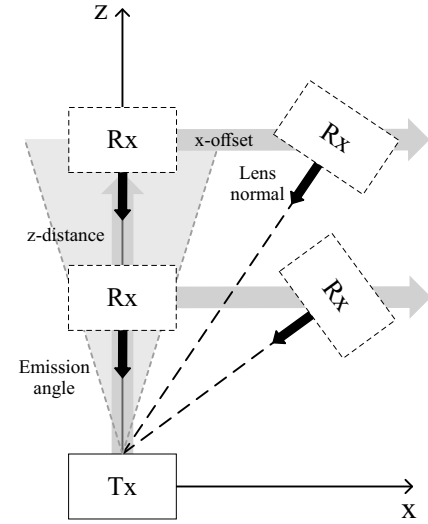


Fig. 4. Schematic view of the experimental setup for coverage measurement of the VCSEL-based transmitter. The dashed Rx boxes depict the movement of the receiver away from the transmitter along the z- and x-axes and its rotation towards the transmitter.

2) Line Coding and Equalizer Measurement Setup: The second setup focused on evaluating the line codes and equalizer considered in Sec. IV-A with the binary VCSEL-based transmitter, additionally including a TDE for comparison. A PIN photodiode-based free-space receiver of the type Femto HSPRX-I-1G4-SI was used, with a 3 dB bandwidth from 10 kHz to 1.4 GHz. The small area ($d = 0.4$ mm) and lack of a lens on this receiver limited the transmission distance to a few centimeters, but its higher bandwidth allows a better assessment of the transmitter properties, compared to the coverage measurement setup. The receiver was placed at a distance of 2.5 cm from the transmitter in order to generate a sufficiently high signal amplitude by capturing the light of all four VCSEL arrays.

Compared to the LED-based frontends in Sec. IV-A, the ratio of the effective high-pass cut-off frequency to the symbol rate tends to be lower when using VCSEL arrays, which relaxes the requirements for line-coding algorithms. In the LED-based setup, this ratio ranges between 1.6 % and 0.1 % for the tested symbol rates from 12.5 to 200 MBd. In the VCSEL-based transmitter, the high-pass cut-off frequency is ≈ 1.6 MHz, and the lowest tested symbol rate was 1 GBd, resulting in a ratio of 0.16 %. Additionally, the VCSEL-

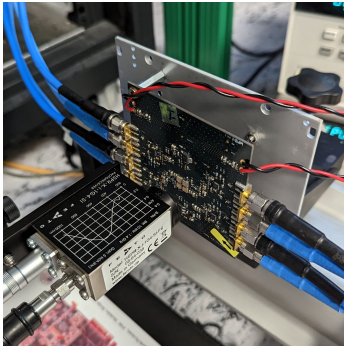


Fig. 5. Photo of the line coding and equalizer measurement setup with the VCSEL-based transmitter prototype and the Femto HSPR-X-I-1G4-SI receiver.

based OFE uses a switching type driver optimized for the transmission of pulsed modulation formats such as OOK, opposed to the linear drivers used in the LED-based frontends. We applied linear equalization to combat the impact of band-pass filtering through the OFEs in both cases. For the VCSEL-based transmitter, this is justified by the fact that relevant band-limiting effects occur on the output side of the switching mode driver.

The symbol rate was varied between 1 GBd and 5 GBd in steps of 250 MBd. Measurements were performed with the line codes 64b66b, 64b67b, and 8b10b. Besides FDE, the 10-tap TDE was also evaluated. The number of bits per transmission was increased to 820,144 to enhance the accuracy of the bit error rate (BER) evaluation.

Due to the 3 dB-bandwidth of the receiver of 1.4 GHz, our setup was still bandwidth-limited by the receiver at symbol rates higher than 2.8 GBd, and the used drivers have a specified limit of 3.2 GBd. Despite this, we could successfully demonstrate transmissions even above these limits, as presented in Sec. V-B2.

3) Bandwidth Measurement Setup: To evaluate the maximum available bandwidth of the VCSEL transmitter, a multi-mode fiber (MMF)-coupled Coherent Solutions matrIQ-O2E 1201 receiver with a bandwidth of 35 GHz was used. To couple a sufficient amount of light into this receiver, an MMF was brought as close as possible to the diffusor on one of the VCSEL arrays of the transmitter. A better coupling could have been achieved without the diffusor in this setup, but the VCSEL arrays and diffusors are packaged together and could not be separated without destroying the assembly, which would also have critically changed the assessment of eye safety. This significantly limited the power detected by the receiver, but a sufficient amount was captured to assess the transmitter bandwidth. The symbol rate was now varied from 1 to 8 GBd. Otherwise, the setup remains unchanged from the one described in the previous section.

Due to the angular dependency and low distance between fiber and diffusor, only the light from one of the four VCSEL arrays was captured by the receiver. As the layout of the board is symmetric, this can be considered sufficient to assess the bandwidth of the electrical circuitry on the transmitter board, though.

V. RESULTS

This section presents the results obtained with the previously described experimental setups. First the results for LED-based OFE prototypes are given. The second subsection presents the results for the transmitter prototype based on VCSEL arrays.

A. LED-based Experiments

This section presents the results obtained using LED-based front-ends described in Sec. IV-A [21]. The aim is to reduce the overhead with different line codes and cyclic prefix lengths. EVM and BER are analyzed for various symbol rates both with and without FDE. As the performance was found to only vary marginally over a distance between 2 and 6 m [21], the evaluation versus distance is not shown here. In conjunction with the BER limit of 3×10^{-4} , the BER serves to show the limitations of the different configurations. The BER limit is equivalent to a block error rate (BLER) of 1×10^{-3} for the RS FEC of the standardized PM-PHY [3]. In several cases no bit error rate could be determined after transmitting $\approx 1 \times 10^6$ bits (i.e., $\text{BER} < 1 \times 10^{-5}$). Therefore, EVM is used as a second metric to evaluate trends for different configurations.

The performance of the different line coding techniques and FDE parameters is shown in Fig. 6 for a distance of 3 m. Fig. 6a presents the EVM for demodulation with and without FDE with a long CP. Without equalization, 8b10b reaches the lowest EVMs, with the results for other line codes being significantly higher, of which 64b67b performs better. The same tendency is visible for equalized transmissions, but the gaps between the codes are much smaller. Furthermore, without equalization, EVM increases significantly both for high and low symbol rates for all codes. This is due to the impact of the high- and low-pass characteristics of the front-ends, described in Sec. IV-A. All coding schemes reach the optimum performance at 25 MBd. Again, this effect is also visible with equalization, but less pronounced, and the point of lowest EVM moves up to 50 MBd for uncoded data and 64b67b.

The BER values in Fig. 6d show the same trend as the EVM curves for uncoded data and 64b67b in the BER. Without equalizer, the guided scrambler 64b67b achieve a BER below the FEC limit for 25 and 50 MBd. For 8b10b, no errors occur below 200 MBd. With the equalizer using the base setting here (long CP, interpolation with $\mathbf{W}_{N_{CP}/2, \widehat{\text{snr}}}^{lmmse}$), no errors are observed with any code at any symbol rate.

Confirming the results in [70], 8b10b improves performance compared to the statistical approaches (64b67b and uncoded data) especially at low symbol rates and when equalization is not used. At low symbol rates, this can be explained by its effective suppression of low frequency signal components, reducing the impact of high-pass filtering and the severity of resulting baseline wander. Most importantly, though, the performance of all coding techniques with FDE is better than that of any of the results without FDE, showing that equalization has a larger effect than line-coding. Accordingly, overhead can be reduced without sacrificing performance by

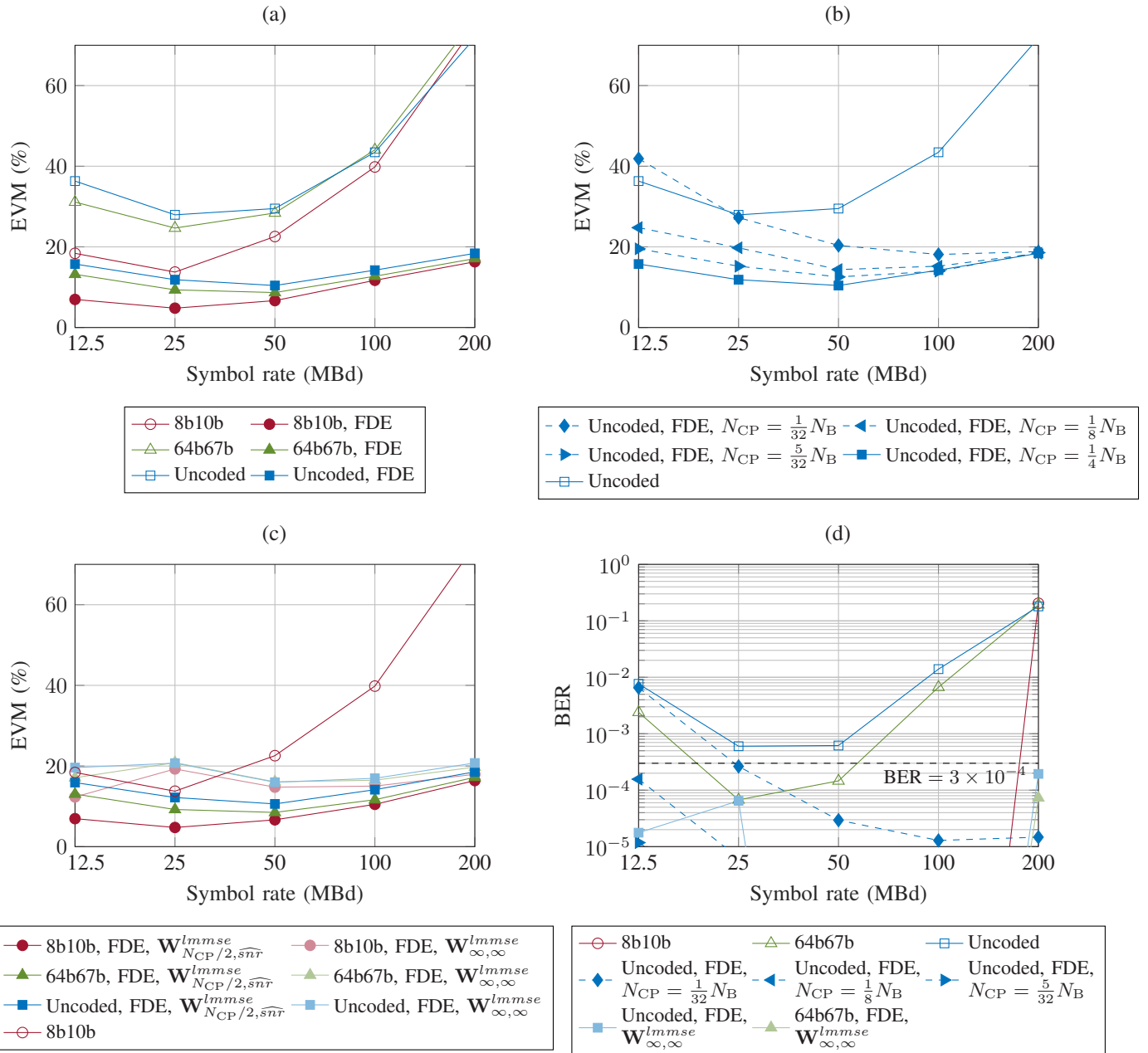


Fig. 6. EVM and BER over symbol rate using LED-based front-ends at 3 m distance: EVM for different line codes (a) with and without FDE, (b) for uncoded data with FDE and different CP lengths, (c) with FDE and the channel response interpolated with $\mathbf{W}^{lmmse}_{N_{CP}/2, \hat{snr}}$ and $\mathbf{W}^{lmmse}_{\infty, \infty}$, and (d) all corresponding BERs. Configurations not exceeding a BER of 1×10^{-5} at any symbol rate are not shown in (d). Where not indicated otherwise, $N_{CP} = \frac{1}{4}N_B$ and $\mathbf{W}^{lmmse}_{N_{CP}/2, \hat{snr}}$ are used for FDE.

omitting 8b10b and using only the equalizer instead. This way, only the CPs cause overhead.

To find potential for further overhead reduction, Fig. 6b shows results with different CP lengths for uncoded random data with FDE. These results indicate that the impact of CP length on the performance of the FDE varies strongly with symbol rate. At low symbol rates, the shorter CPs significantly increase the EVM values. With increasing symbol rate, the difference vanishes. At 12.5 MBd, the EVM with the shortest CP ($N_{CP} = \frac{1}{32}N_B$), as defined in the standard as “*short CP*”, even exceeds that of the uncoded, unequalized transmission, while the BER (Fig. 6d) is only slightly lower. With increasing

CP length, EVM decreases and approaches that of the “*long CP*” in the standard with $N_{CP} = \frac{1}{4}N_B$. The largest change results from the step to $N_{CP} = N_B/8$. Another significant improvement is visible for the step to $N_{CP} = \frac{5}{32}N_B$.

Accordingly, high-pass filtering is the limiting factor for CP length, which is corroborated by the point of lowest EVM moving up to 100 MBd for the short CP. This is explained by the baseline wander: At lower symbol rates, more signal components are present at lower frequencies, and stronger baseline wander results. This leads to “*inter-block interference*”, as the baseline wander caused by one signal block extends beyond the length of the CP of the following block and disturbs its

pseudo-cyclic structure, causing a penalty in the FDE. But even for the shortest CP, the BER is still below 3×10^{-4} at 25 MBd and above. $N_{CP} = \frac{1}{8}N_B$ suffices to eliminate bit errors at all symbol rates larger than 12.5 MBd, and the BER limit of 3×10^{-4} is met at all symbol rates, making this a favorable choice. With that, overhead is reduced from 25 to 12.5 % compared to unequalized 8b10b transmission, and even from 56.25 %, compared to the combination of 8b10b with long CPs. At high symbol rates over 50 MBd, the CP length and line coding choice have minor impact. These results indicate that additional CP length options are recommendable in future standards.

Finally, Fig. 6c demonstrates the impact of channel interpolation when using FDE with the interpolation matrix $\mathbf{W}_{N_{CP}/2, \widehat{snr}}^{lmmse}$, used for the results discussed above, and the simplified matrix $\mathbf{W}_{\infty, \infty}^{lmmse}$, introduced in Sec. III-B2. The EVM values show that at high symbol rates, there is virtually no penalty when using the simplified method. At symbol rates of 50 MBd and below, the EVM is notably higher than the baseline, with an uptick at 25 MBd. At this point, the EVM also exceeds that of unequalized transmission with 8b10b. Note that the channel estimation sequence is different at each symbol rate and may be unfavorable at 25 MBd, causing the observed uptick. This may be solved by selecting a different sequence from the set of Gold sequences of the corresponding length. Nonetheless, all observed BERs (Fig. 6d) are below the BER threshold of 3×10^{-4} , with errors only occurring for uncoded data below 50 MBd and above 100 MBd, and for 64b67b at 200 MBd, making FDE with simplified interpolation a potential candidate for replacing 8b10b.

B. VCSEL-based Experiments

This section investigates the use of OOK for non-directed OWC based on VCSEL-arrays, as described in Sec. IV-B. First, the coverage of our transmitter is studied [22], then the impact of line code and equalizer [23], and finally the transmitter's bandwidth limitations. Because the PM-PHY is only defined up to 200 MBd in IEEE Std 802.15.13-2023, higher bandwidths need to be defined in future versions. Instead of the RS FEC, we anticipate future use of advanced FEC here and set the BER limit as 4.5×10^{-3} for a block error rate (BLER) of 1×10^{-3} when using a low-density parity check (LDPC) FEC with 5 % overhead and a block size of 4320 bits [79].

1) *Coverage Measurements:* Fig. 7 shows BER values observed in the coverage measurement setup over x-offset at a z-distance of 2.5 m for the symbol rates 2 and 2.5 GBd. No bit errors occurred at 1 and 1.5 GBd. At 2 GBd, with the equalizer all observed BERs were still below the lower y-axis limit of 1×10^{-4} , which is why the corresponding points do not appear in the figure. This limit was chosen due to the relatively low number of transmitted bits (65,536). For 2 GBd, also the results without equalizer are within the BER limit. The plots for 2 GBd without FDE and 2.5 GBd with FDE show a drop in the error level with a minimum between the offsets 0.6 m and 0.8 m. This is due to the distribution of optical power in the emission cone of the VCSEL arrays: For

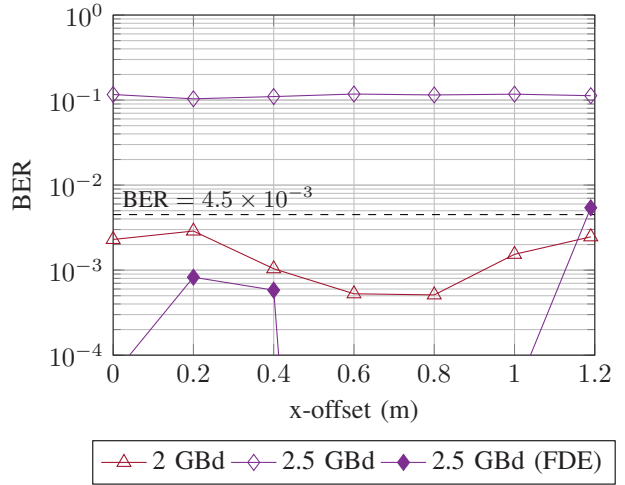


Fig. 7. BER for the VCSEL transmitter over x-offset at a z-distance of 2.5 m. Observed values for the 2 GBd measurement with FDE were all smaller than 1×10^{-4} and are thus not shown in the figure.

gain-guided laser diodes, a noticeable concentration of optical power typically occurs towards the edges of the emission cone due to the superposition of multiple spatial modes [80], which is why the performance first improves for increasing offsets, and then finally deteriorates around 1 m offset. This drop is not visible in the results for 2.5 GBd without FDE, because the performance in this case is limited by the low bandwidth of the receiver (1 GHz). Since the full width emission angle of the diffusors in the y-direction (45°) is 75 % of the angle in the x-direction (60°), this results in a total covered area amounting to $2 \cdot 1.2 \text{ m} \cdot 2 \cdot 0.75 \cdot 1.2 \text{ m} = 4.32 \text{ m}^2$ in which the BER limit is fulfilled. At 2.5 GBd the limit is maintained up to at an offset of 1 m, but only with the equalizer, in this case resulting in a covered area of 3 m^2 .

2) *Impact of Line Coding and Equalizer:* The following experiments focus on exploring different line-codes and equalizers, as described in Sec. III, with the binary VCSEL-based transmitter for a wide range of symbol rates, using the experimental setup described in Sec. IV-B2.

Fig. 8a shows EVM values for symbol rates from 1 to 5 GBd. The EVM without equalizer increases almost linearly with increasing symbol rate, while it remains flat with TDE and FDE for the lower symbol rates and increases above 2.75 GBd, which is approximately twice the receiver bandwidth (1.4 GHz). Remarkably, the EVM does not reflect significant differences between the different coding schemes. Without equalization and at symbol rates below 2.75 GBd, 8b10b slightly outperforms the other schemes, similar to the LED-based system (Sec. V-A). This is intuitive due to the higher rate of symbol transitions in the 8b10b encoded data stream, which reduces distortion due to high-pass effects at low symbol rates. With equalization, the differences between line codes are insignificant. This is also reflected in BER values in Fig. 8b, i.e., the effect of equalization outweighs the effect of line-coding. The results are barely distinguishable between different line codes for the transmissions with either equalizer, with the first errors appearing only at 3.5 GBd. With TDE, the only significant change appears at very high symbol

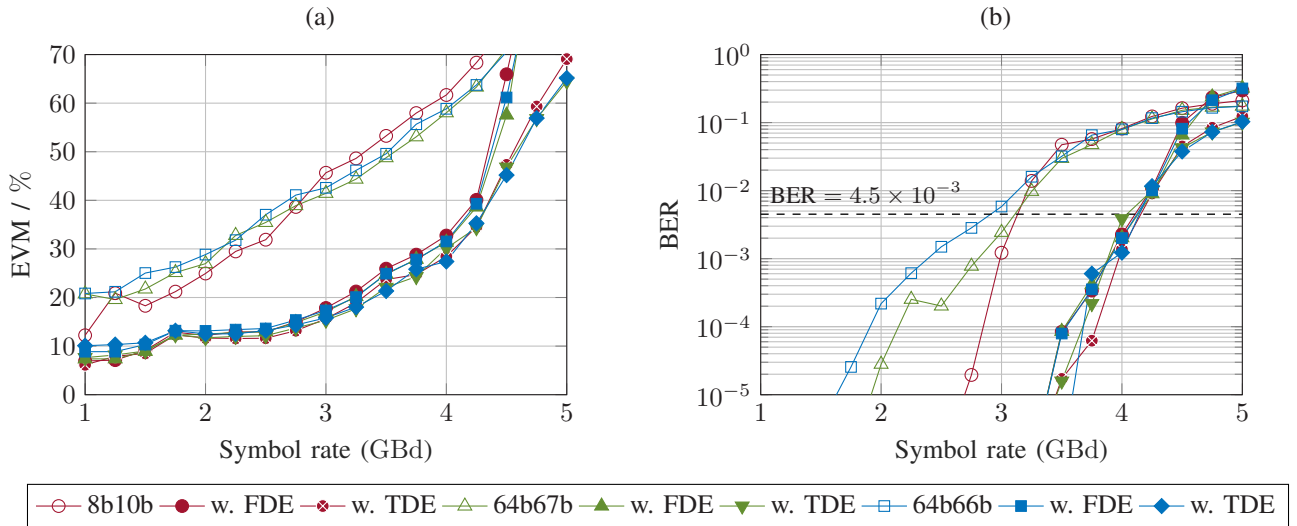


Fig. 8. (a) EVM and (b) BER for the VCSEL transmitter line-coding and equalizer comparison over symbol rate with the Femto HSPR-X-I-1G4-SI receiver.

rates between 4 and 5 GBd, where it achieves a lower BER than FDE, but well above the FEC limit. With either equalizer, for all line codes the BER threshold is crossed at 4.25 GBd. Without equalizer, larger differences are notable, but only at lower symbol rates. The BER for 64b66b increases steadily after first errors appear at 1.75 GBd, and crosses the threshold at 3 GBd. For 8b10b, first errors appear at 2.75 GBd, and the BER threshold is crossed at 3.25 GBd. 64b67b lies between the two and crosses the threshold at 3.25 GBd, as well.

The main limitation in this setup is the band-limiting receiver. Including the overhead factors described in Sec. III, following net data rates R_{data} are reached, according to (1): 4 Gbit/s for the combination of TDE and 64b66b, as both do not cause overhead. Using FDE with the CP length of $N_{\text{CP}} = N_B/8$ and/or another line code than 64b66b decrease the throughput due to added overhead, down to 2.84 Gbit/s for FDE with 8b10b. Without equalization, maximum throughputs of 2.4, 2.75, and 2.87 Gbit/s are possible for 8b10b, 64b66b and 64b67b, respectively.

These results indicate that the schemes defined in the IEEE 802.15.13-2023 PM-PHY for LED-based OWC, namely 8b10b line coding and frequency domain equalization, may not generally be required for high bandwidth VCSEL-based OWC, where the highest throughput is achieved with a simple scrambler and time-domain equalization. The optimal line coding depends on the system design: For maximum throughput above 3 Gbit/s, the 64b66b line code and equalization are favorable. If compatibility with OFDM is wanted, for example in IEEE Std 802.15.13-2023, FDE is the best choice. TDE only eliminates the overhead due to the CPs. To maximize energy efficiency, a configuration without equalizer still reaches 2.87 Gbit/s with 64b67b line-coding. 8b10b reduces the achievable throughput without equalizer to 2.4 Gbit/s, but increases tolerance for higher high-pass cut-off frequencies on the receiver side (see Sec. V-A), e.g., for the APD receiver used in the setup described in Sec. IV-B1 that has a cut-off frequency of 5 MHz.

3) *Bandwidth Evaluation:* Fig. 9 shows the results from the transmitter bandwidth evaluations using the Coherent Solutions receiver with 35 GHz bandwidth for the 64b66b line-coding with and without TDE. For reference, the results based on the Femto receiver with 1.4 GHz bandwidth that were presented in the previous section are shown in gray.

The EVM values in Fig. 9a make the removal of the bandwidth limitation caused by the Femto receiver visible. Instead of a steep increase starting at 1 GBd, the EVM without equalizer stays below 30% up to 3.75 GBd for the high-bandwidth receiver, and only then steadily rises. With TDE, EVM readings start slightly higher than with the Femto receiver, but stay below $\approx 15\%$ before steadily climbing after 3 GBd. Overall, the EVM values of equalized and non-equalized transmissions differ less than with the Femto receiver. The observed BER values shown in Fig. 9b align very well with the EVM findings. The BER limit of 4.5×10^{-3} is now fulfilled up to 4.25 GBd, both with and without the equalizer. This means that the data rate is increased by more than 50% when using a faster receiver without the equalizer. With the equalizer, the data rate increases only slightly from 4 to 4.25 GBd.

Based on these findings, the need for an equalizer arises from band limitations on the receiver side. Note that due to the need to reduce parasitic capacitance, a faster receiver has a smaller active area, which will often not capture enough light for LiFi applications. The equalizer helps to overcome bandwidth limitations when using large-area receivers that capture more light. Nonetheless, the area of the 1.4 GHz receiver is also relatively small and it would need a lens forming a narrow beam to be directed towards the transmitter in a LiFi setting. This is an important difference between LED-based and VCSEL-based LiFi systems: While LED-based LiFi has limited bandwidth and can use larger receivers, VCSEL-based LiFi needs receivers with smaller area to overcome bandwidth limitations. This highlights the importance of developing high-bandwidth receivers with high sensitivity and automated beam tracking, which remains a subject of further research towards

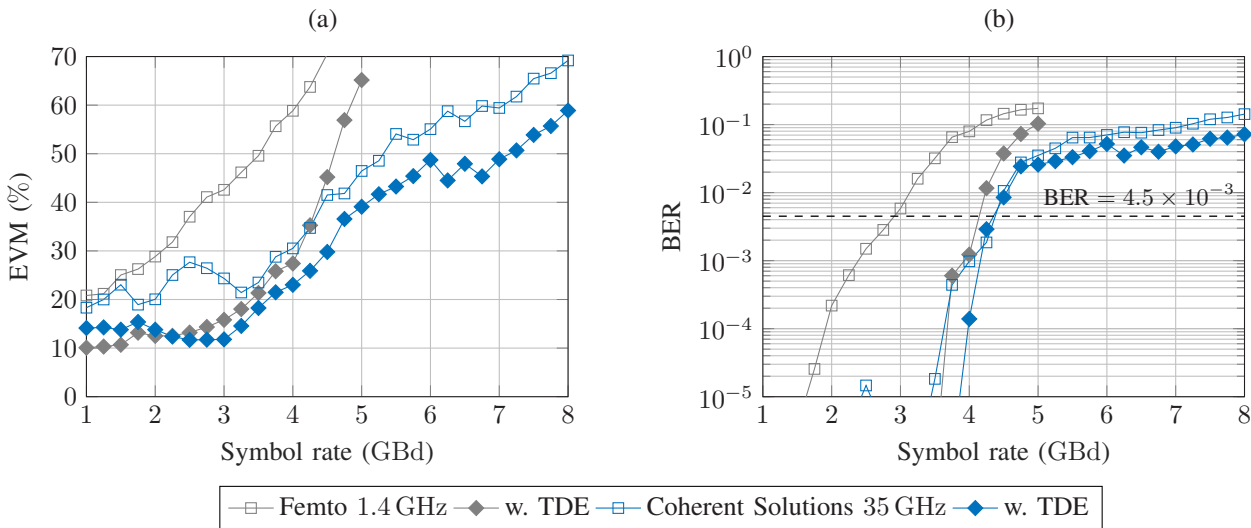


Fig. 9. (a) EVM and (b) BER for the VCSEL transmitter bandwidth evaluation with the Coherent Solutions matrIQ-O2E 1201 receiver over symbol rate with the 64b66b scrambler. Results from the line-coding and equalizer evaluation up to 5 GBd with the Femto HSPR-X-I-1G4-SI receiver (Sec. V-B2) are shown for reference.

new LiFi applications with higher bandwidth.

VI. CONCLUSIONS

This paper provides an extensive analysis of potential enhancements to the Pulsed Modulation PHY (PM-PHY) for optical wireless communication (OWC) defined in IEEE Std 802.15.13-2023 and demonstrates a newly developed vertical-cavity surface-emitting laser (VCSEL) transmitter for multi-Gbit/s on-off keying (OOK) transmission.

As an alternative to the common 8b10b, the scrambler-based 64b66b and 64b67b line codes can significantly reduce the overhead with minor impact on the performance. When using frequency domain equalization (FDE), the length of the cyclic prefix (CP) and interpolation of the channel frequency response have a large impact on system performance. Measurements with a light-emitting diode (LED)-based setup demonstrate that the 8b10b line code, which introduces an overhead of 25 %, can be replaced with an effective equalizer. The FDE enables symbol rates down to 12.5 MBd, countering high-pass filtering, as well as up to 200 MBd, where low-pass effects dominate. However, the performance results indicate that further options besides the currently defined CP lengths in IEEE Std 802.15.13-2023 may be beneficial as the current ones are either too long, reducing efficiency, or too short, causing inter-block interference.

Measurements with a VCSEL-based transmitter prototype eliminate overhead by replacing FDE with time domain equalization (TDE) to reach data rates up to 4 Gbit/s in a setup with a band-limited receiver. Without band-limitation, the transmitter reaches 4.25 Gbit/s also without equalizer. Coverage measurements show that the transmitter can serve an area of 4.32 m^2 at a distance of 2.5 m, confirming that a practical deployment in LiFi systems is viable.

Overall, these enhancements largely remove the overhead of the PM-PHY for OWC with OOK, which provides high energy efficiency and maximizes reach, as known from fiber-optic systems. In the context of laser-based OWC, pushing

for higher bandwidth instead of higher modulation order allows power-efficient digital driver circuits similar to fiber-optics. VCSEL-arrays from sensing applications are a practical replacement for high-power LEDs, as they can provide higher bandwidth at similar power levels for multi-Gbit/s LiFi. An open research topic is the development of receivers with high bandwidth, high sensitivity, and automated beam tracking to detect these signals in a non-directed LiFi system.

REFERENCES

- [1] J. M. Kahn and J. R. Barry, "Wireless infrared communications," *Proceedings of the IEEE*, vol. 85, no. 2, pp. 265–298, 1997.
- [2] J. Grubor, V. Jungnickel, and K.-D. Langer, "Capacity analysis in indoor wireless infrared communication using adaptive multiple subcarrier transmission," in *Proceedings of 2005 7th International Conference Transparent Optical Networks (ICTON), 2005.*, Jul. 2005, pp. 171–174, We.C2.7.
- [3] M. Hinrichs, P. Wilke Berenguer, J. Hilt, P. Hellwig, D. Schulz, A. Paraskevopoulos, K. L. Bober, R. Freund, and V. Jungnickel, "A physical layer for low power optical wireless communications," *IEEE Trans. Green Commun. Netw.*, vol. 5, no. 1, pp. 4–17, Nov. 2020, date of issue: March 2021.
- [4] N. Ledentsov, L. Chorchos, V. Shchukin, V. Kalosha, J. P. Turkiewicz, and N. N. Ledentsov, "Development of VCSELs and VCSEL-based Links for Data Communication beyond 50Gb/s," in *2020 Optical Fiber Communications Conference and Exhibition (OFC)*, Mar. 2020, p. M2A.3.
- [5] J. R. García-Meré, J. Rodríguez, D. G. Lamar, and J. Sebastián, "On the Use of Class D Switching-Mode Power Amplifiers in Visible Light Communication Transmitters," *Sensors*, vol. 22, no. 13, p. 4858, Jan. 2022.
- [6] J. L. Wei, J. D. Ingham, D. G. Cunningham, R. V. Penty, and I. H. White, "Performance and Power Dissipation Comparisons Between 28 Gb/s NRZ, PAM, CAP and Optical OFDM Systems for Data Communication Applications," *J. Lightw. Technol.*, vol. 30, no. 20, pp. 3273–3280, Oct. 2012.
- [7] IEEE Computer Society, *Part 3: Carrier Sense Multiple Access with Collision Detection (CSMA/CD) Access Method and Physical Layer Specifications, Amendment: Media Access Control (MAC) Parameters, Physical Layers, and Management Parameters for 10 Gb/s Operation*, IEEE Std. 802.3ae-2002, Jun. 2002.
- [8] A. Street, K. Samaras, D. O'Brien, and D. Edwards, "Closed form expressions for baseline wander effects in wireless IR applications," *Electronics Letters*, vol. 33, no. 12, pp. 1060–1062, Jun. 1997.

- [9] A. Hayes, Z. Ghassemlooy, and N. Seed, "The effect of baseline wander on the performance of digital pulse interval modulation," in *IEE Colloquium on Optical Wireless Communications (Ref. No. 1999/128)*, Jun. 1999, pp. 13/1–13/5.
- [10] A. X. Widmer and P. A. Franaszek, "A DC-balanced, partitioned-block, 8B/10B transmission code," *IBM Journal of Research and Development*, vol. 27, no. 5, pp. 440–451, Sep. 1983.
- [11] I. J. Fair, W. D. Grover, W. A. Krzymien, and R. I. MacDonald, "Guided scrambling: a new line coding technique for high bit rate fiber optic transmission systems," *IEEE Trans. Commun.*, vol. 39, no. 2, pp. 289–297, Feb. 1991.
- [12] J. Saadé, A. Goulahtsen, A. Picco, J. Huloux, and F. Pétrot, "Low overhead, DC-Balanced and run length limited Line Coding," in *2015 IEEE 19th Workshop on Signal and Power Integrity (SPI)*, May 2015, pp. 1–4.
- [13] L. Grobe, V. Jungnickel, K.-D. Langer, M. Haardt, and M. Wolf, "On the impact of highpass filtering when using PAM-FDE for visible light communication," in *IEEE Wireless Communications and Networking Conference Workshops (WCNCW)*. IEEE, Apr. 2016.
- [14] M. Wolf and M. Haardt, "On the DC balance of multi-level PAM VLC systems," in *2019 21st International Conference on Transparent Optical Networks (ICTON)*. IEEE, Jul. 2019.
- [15] 802.15 WG - Wireless Specialty Networks (WSN) Working Group, *IEEE 802.15.13-2023: IEEE Approved Draft Standard for Multi-Gigabit per Second Optical Wireless Communications (OWC), with Ranges up to 200 meters, for both stationary and mobile devices*, IEEE Std., 2023.
- [16] M. Hinrichs, C. Schmidt, B. Poddig, J. Hilt, P. Hellwig, D. Schulz, K. L. Bober, J. Schostak, R. Freund, and V. Jungnickel, "Demonstration of optical wireless communications using the pulsed modulation PHY in IEEE 802.15.13," in *2020 22nd International Conference on Transparent Optical Networks (ICTON)*. IEEE, Jul. 2020, pp. 1–4.
- [17] Telecommunication Standardization Sector of ITU, *Recommendation ITU-T G.9960: Unified high-speed wireline-based home networking transceivers (G.hn) – System architecture and physical layer specification*, ITU-T Std., Nov. 2018.
- [18] ———, *Recommendation ITU-T G.9991: High speed indoor visible light communication transceiver – System architecture, physical layer and data link layer specification*, ITU-T Std., Mar. 2019.
- [19] 802.11 WG - Wireless LAN Working Group, *IEEE Standard for Information Technology—Telecommunications and Information Exchange between Systems - Local and Metropolitan Area Networks—Specific Requirements - Part 11: Wireless LAN Medium Access Control (MAC) and Physical Layer (PHY) Specifications*, IEEE Std., 2007.
- [20] A. A. Zaidi, R. Baldemair, V. Moles-Cases, N. He, K. Werner, and A. Cedergren, "OFDM Numerology Design for 5G New Radio to Support IoT, eMBB, and MBSFN," *IEEE Communications Standards Magazine*, vol. 2, no. 2, pp. 78–83, Jun. 2018.
- [21] M. Hinrichs, B. Poddig, P. Hellwig, and V. Jungnickel, "Reducing overhead for low-power optical wireless communications," in *IECON 2022–48th Annual Conference of the IEEE Industrial Electronics Society*. IEEE, Oct. 2022, pp. 1–5.
- [22] M. Hinrichs, G. Boniello, P. Hellwig, D. Schulz, C. Kottke, M. Schubert, R. Böhnke, W. Xu, R. Freund, and V. Jungnickel, "Demonstration of 1.75 Gbit/s VCSEL-based non-directed optical wireless communications with OOK and FDE," in *European Conference and Exhibition on Optical Communication*. Optical Publishing Group, Sep. 2022, p. We5.52.
- [23] M. Hinrichs, M. Silveira, G. Boniello, D. Schulz, M. Schubert, R. Böhnke, W. Xu, R. Freund, and V. Jungnickel, "4 Gbit/s optical wireless communication with high-power transmitter," in *49th European Conference on Optical Communications (ECOC 2023)*, Oct. 2023, pp. 1290–1293.
- [24] M. Hinrichs, J. Hilt, V. Jungnickel, S.-K. Lim, I. S. Jang, J.-D. Jeong, and M. Noshad, "Pulsed modulation PHY for power efficient optical wireless communication," in *IEEE International Conference on Communications (ICC)*. IEEE, May 2019.
- [25] M. Hinrichs, W. Costa, H. Rocha, M. Pontes, M. Segatto, A. Paraskevopoulos, V. Jungnickel, R. Freund, and J. Silva, "A performance comparison of OFDM and pulsed PHY modulations in optical wireless communications," in *2023 South American Conference On Visible Light Communications (SACVLC)*, Nov. 2023, pp. 124–129.
- [26] Telecommunication Standardization Sector of ITU, *Recommendation ITU-T G.987.2: 10-Gigabit-capable passive optical networks (XG-PON): Physical media dependent (PMD) layer specification*, ITU-T Std., Jun. 2023.
- [27] I. D. A. (IrDA), *Infrared Data Association Serial Infrared Physical Layer Specification*, Infrared Data Association (IrDA) Std. 1.4, May 2001.
- [28] J. Armstrong and B. Schmidt, "Comparison of asymmetrically clipped optical OFDM and DC-biased optical OFDM in AWGN," *IEEE Commun. Lett.*, vol. 12, no. 5, pp. 343–345, May 2008.
- [29] M. Wolf, S. A. Cheema, and M. Haardt, "Block Transmission with Frequency Domain Equalization for VLC," in *Optical Wireless Communications: An Emerging Technology*, ser. Signals and Communication Technology, M. Uysal, C. Capsoni, Z. Ghassemlooy, A. Boucouvalas, and E. Udvari, Eds. Cham: Springer International Publishing, 2016, pp. 299–323.
- [30] V. Jungnickel, J. Hohmann, D. Schulz, P. Hellwig, J. Hilt, C. Kottke, and R. Freund, "Laser-based LiFi for 6G: Potential and Applications," in *The 9th Laser Display and Lighting Conference 2020 (LDC 2020)*, Sep. 2020.
- [31] H. Ochiai and H. Imai, "On the distribution of the peak-to-average power ratio in OFDM signals," *IEEE Trans. Commun.*, vol. 49, no. 2, pp. 282–289, Feb. 2001.
- [32] S. Dimitrov, S. Sinanovic, and H. Haas, "Signal Shaping and Modulation for Optical Wireless Communication," *J. Lightw. Technol.*, vol. 30, no. 9, pp. 1319–1328, May 2012.
- [33] D. J. F. Barros, S. K. Wilson, and J. M. Kahn, "Comparison of orthogonal frequency-division multiplexing and pulse-amplitude modulation in indoor optical wireless links," *IEEE Trans. Commun.*, vol. 60, no. 1, pp. 153–163, Jan. 2012.
- [34] A. Nuwanpriya, S.-W. Ho, J. Zhang, A. Grant, and L. Luo, "PAM-SCFDE for optical wireless communications," *J. Lightw. Technol.*, pp. 2938–2949, 2015.
- [35] J. Lian, M. Noshad, and M. Brandt-Pearce, "Comparison of Optical OFDM and M-PAM for LED-Based Communication Systems," *IEEE Commun. Lett.*, vol. 23, no. 3, pp. 430–433, Mar. 2019.
- [36] S. Mardanikorani, X. Deng, and J.-P. M. G. Linnartz, "Optimization and Comparison of M-PAM and Optical OFDM Modulation for Optical Wireless Communication," *IEEE Open J. Commun. Soc.*, vol. 1, pp. 1721–1737, 2020.
- [37] M. Wolf and M. Haardt, "A review of advanced modulation schemes for band limited wireless optical systems based on intensity modulation and direct detection," in *2024 24th International Conference on Transparent Optical Networks (ICTON)*, Jul. 2024, pp. 1–7.
- [38] N. Chi, M. Zhang, Y. Zhou, and J. Zhao, "3.375-Gb/s RGB-LED based WDM visible light communication system employing PAM-8 modulation with phase shifted Manchester coding," *Optics Express*, vol. 24, no. 19, p. 21663, Sep. 2016.
- [39] K. M. V. D. Zwag, M. P. Marinho, W. D. S. Costa, F. De Assis Souza Dos Santos, T. F. Bastos-Filho, H. R. O. Rocha, M. E. V. Segatto, and J. A. L. Silva, "A Manchester-OOK Visible Light Communication System for Patient Monitoring in Intensive Care Units," *IEEE Access*, vol. 9, pp. 104217–104226, 2021.
- [40] L. Grobe and K.-D. Langer, "Block-based PAM with frequency domain equalization in visible light communications," in *IEEE Globecom Workshops (GC Wkshps)*. IEEE, Dec. 2013.
- [41] D. Falconer, S. L. Ariyavisitakul, A. Benyamin-Seeyar, and B. Eidson, "Frequency domain equalization for single-carrier broadband wireless systems," *IEEE Commun. Mag.*, vol. 40, no. 4, pp. 58–66, Apr. 2002.
- [42] A. Surampudi, R. Singh, A. Riaz, W. Ali, G. Faulkner, D. C. O'Brien, and S. Collins, "A Digital Pre-equalizer for Optical Wireless Links," *J. Lightw. Technol.*, pp. 1–1, 2021.
- [43] S. Dimitrov, S. Sinanovic, and H. Haas, "Clipping noise in OFDM-based optical wireless communication systems," *IEEE Trans. Commun.*, vol. 60, no. 4, pp. 1072–1081, Apr. 2012.
- [44] Y. Celik, R. C. Kizilirmak, N. Odabasioglu, and M. Uysal, "On the performance of SC-FDE schemes with decision feedback equalizer for visible light communications," in *2015 17th International Conference on Transparent Optical Networks (ICTON)*, Jul. 2015, pp. 1–4.
- [45] T. Kamalakis, J. W. Walewski, G. Ntogiari, and G. Mileounis, "Empirical Volterra-Series Modeling of Commercial Light-Emitting Diodes," *J. Lightw. Technol.*, vol. 29, no. 14, pp. 2146–2155, Jul. 2011.
- [46] S. Mardani, A. Alexeev, and J.-P. Linnartz, "Modeling and compensating dynamic nonlinearities in LED photon-emission rates to enhance OWC," in *Light-Emitting Devices, Materials, and Applications*, vol. 10940. SPIE, Mar. 2019, pp. 113–130.
- [47] G. Stepienak, J. Siuzdak, and P. Zwierko, "Compensation of a VLC phosphorescent white LED nonlinearity by means of Volterra DFE," *IEEE Photon. Technol. Lett.*, vol. 25, no. 16, pp. 1597–1600, 2013.
- [48] A. A. Purwita, C. Chen, M. Safari, and H. Haas, "Cyclic-Prefixed System with PAM using DFE and THP for Uplink Transmission in LiFi," in *ICC 2019 - 2019 IEEE International Conference on Communications (ICC)*, May 2019, pp. 1–6.

- [49] D. Schulz, P. W. Berenguer, J. Hilt, P. Hellwig, A. Paraskevopoulos, R. Freund, and V. Jungnickel, "Use Cases for Optical Wireless Communication," in *2018 Optical Fiber Communications Conference and Exposition (OFC)*, Mar. 2018, pp. 1–3.
- [50] P. Wilke Berenguer, P. Hellwig, D. Schulz, J. Hilt, G. Kleinpeter, J. K. Fischer, and V. Jungnickel, "Real-time optical wireless mobile communication with high physical layer reliability," *J. Lightw. Technol.*, vol. 37, no. 6, pp. 1638–1646, Mar. 2019.
- [51] C. Lee, M. S. Islim, S. Videv, A. Sparks, B. Shah, P. Rudy, M. McLaurin, H. Haas, and J. Raring, "Advanced LiFi technology: Laser light," in *Light-Emitting Devices, Materials, and Applications XXIV*, vol. 11302. SPIE, Feb. 2020, pp. 116–123.
- [52] C. Kottke, C. Caspar, V. Jungnickel, R. Freund, M. Agustin, J. R. Kropf, and N. N. Ledentsov, "High-Speed DMT and VCSEL-Based MMF Transmission Using Pre-Distortion," *J. Lightw. Technol.*, vol. 36, no. 2, pp. 168–174, Jan. 2018.
- [53] N. Ledentsov, C. Kottke, L. Chorchos, V. Shchukin, O. Y. Makarov, M. B. Sanayeh, V. Kalosha, V. Jungnickel, R. Freund, J. P. Turkiewicz, and N. N. Ledentsov, "Up to 600 Gbit/s data transmission over 100 m of single multi-mode fiber using $4 \times \lambda$ 850–940 nm VCSELs," in *2022 Optical Fiber Communications Conference and Exhibition (OFC)*, Mar. 2022, pp. 1–3.
- [54] O. Bouchet, M. Lanoiselée, D. O'Brien, R. Singh, M. Ghoraishi, R. Perez, V. Guerra, S. Topsu, and J. Garcia-Marquez, "Terabit per second optical wireless links for virtual reality technology," in *Laser Communication and Propagation through the Atmosphere and Oceans VII*, vol. 10770. SPIE, Sep. 2018, pp. 51–59.
- [55] Z. Wei, S. Zhang, S. Mao, L. Wang, L. Zhang, C.-J. Chen, M.-C. Wu, Y. Dong, L. Wang, Y. Luo, and H. Y. Fu, "Full-duplex high-speed indoor optical wireless communication system based on a micro-LED and VCSEL array," *Optics Express*, vol. 29, no. 3, pp. 3891–3903, Feb. 2021.
- [56] S. Liverman, H. Bialek, A. Natarajan, and A. X. Wang, "VCSEL Array-Based Gigabit Free-Space Optical Femtocell Communication," *J. Lightw. Technol.*, vol. 38, no. 7, pp. 1659–1667, Apr. 2020.
- [57] C. Lee, M. S. Islim, S. Das, A. Spark, S. Videv, P. Rudy, B. Shah, M. McLaurin, H. Haas, and J. Raring, "26 Gbit/s LiFi System With Laser-Based White Light Transmitter," *J. Lightw. Technol.*, vol. 40, no. 5, pp. 1432–1439, Mar. 2022.
- [58] I. N. O. Osahon, S. Rajbhandari, I. Kostakis, A. Ihsan, D. Powell, W. Meredith, M. Missous, H. Haas, and J. Tang, "Experimental Demonstration of 38 Gbps Over 2.5 m OWC Systems With Eye-Safe 850 nm SM-VCSELs," *IEEE Photon. Technol. Lett.*, vol. 36, no. 3, pp. 139–142, Feb. 2024.
- [59] J. Hu, F. Hu, J. Jia, G. Li, J. Shi, J. Zhang, Z. Li, N. Chi, S. Yu, and C. Shen, "46.4 Gbps visible light communication system utilizing a compact tricolor laser transmitter," *Optics Express*, vol. 30, no. 3, p. 4365, Jan. 2022.
- [60] P. A. Loureiro, G. M. Fernandes, S. F. H. Correia, R. A. S. Ferreira, F. P. Guiomar, and P. P. Monteiro, "30 Gbit/s Visible Light Communication System with Optimized Color Temperature," in *2024 Optical Fiber Communications Conference and Exhibition (OFC)*, Mar. 2024, pp. 1–3.
- [61] P. A. Loureiro, F. P. Guiomar, and P. P. Monteiro, "25G+ Distance-Adaptive Visible Light Communications Enabled by Entropy Loading," in *2023 Optical Fiber Communications Conference and Exhibition (OFC)*, Mar. 2023, pp. 1–3.
- [62] A. Gomez, K. Shi, C. Quintana, R. Maher, G. Faulkner, P. Bayvel, B. C. Thomsen, and D. O'Brien, "Design and Demonstration of a 400 Gb/s Indoor Optical Wireless Communications Link," *J. Lightw. Technol.*, vol. 34, no. 22, pp. 5332–5339, Nov. 2016.
- [63] T. Koonen, F. Gomez-Agis, F. Huijskens, K. A. Mekonnen, Z. Cao, and E. Tangdiongga, "High-Capacity Optical Wireless Communication Using Two-Dimensional IR Beam Steering," *J. Lightw. Technol.*, vol. 36, no. 19, pp. 4486–4493, Oct. 2018.
- [64] H. Chun, A. Gomez, C. Quintana, W. Zhang, G. Faulkner, and D. O'Brien, "A Wide-Area Coverage 35 Gb/s Visible Light Communications Link for Indoor Wireless Applications," *Scientific Reports*, vol. 9, no. 1, p. 4952, Mar. 2019.
- [65] Y. Ghasempour, C. R. C. M. da Silva, C. Cordeiro, and E. W. Knightly, "IEEE 802.11ay: Next-Generation 60 GHz Communication for 100 Gb/s Wi-Fi," *IEEE Commun. Mag.*, vol. 55, no. 12, pp. 186–192, Dec. 2017.
- [66] W. Wu, N. Cheng, N. Zhang, P. Yang, K. Aldubaikhy, and X. Shen, "Performance Analysis and Enhancement of Beamforming Training in 802.11ad," *IEEE Trans. Veh. Technol.*, vol. 69, no. 5, pp. 5293–5306, May 2020.
- [67] K. Bera, R. Parthiban, and N. Karmakar, "Coverage Improvement of Laser Diode-Based Visible Light Communication Systems Using an Engineered Diffuser," *IEEE Access*, vol. 11, pp. 122 833–122 841, 2023.
- [68] Y. Tang, Z. Fu, R. Yang, H. Zhao, J. Qiu, and K. Liu, "Long-range high-speed laser imaging based on VCSEL array and MPPC array," *Optics Express*, vol. 30, no. 13, p. 23734, Jun. 2022.
- [69] K. L. Bober, S. M. Mana, M. Hinrichs, S. M. Kouhini, C. Kottke, D. Schulz, C. Schmidt, R. Freund, and V. Jungnickel, "Distributed Multiuser MIMO for LiFi in Industrial Wireless Applications," *J. Lightw. Technol.*, vol. 39, no. 11, pp. 3420–3433, Jun. 2021.
- [70] M. Hinrichs, B. Poddig, M. Nölle, P. Hellwig, R. Freund, and V. Jungnickel, "Efficient line coding for low-power optical wireless communications," in *2021 IEEE 94th Vehicular Technology Conference (VTC2021-Fall)*. IEEE, Sep. 2021, pp. 1–7.
- [71] Cortina Systems and Cisco Systems, "Interlaken Protocol Definition," 2008, accessed: 2023-01-24. [Online]. Available: http://interlakenalliance.com/wp-content/uploads/2019/12/Interlaken_Protocol_Definition_v1.2.pdf
- [72] R. Gold, "Optimal binary sequences for spread spectrum multiplexing (corresp.)," *IEEE Trans. Inf. Theory*, vol. 13, no. 4, pp. 619–621, Oct. 1967.
- [73] S. Schiffermüller and V. Jungnickel, "Practical Channel Interpolation for OFDMA," in *IEEE Globecom 2006*, Nov. 2006, pp. 1–6.
- [74] Laser Components, "940nm 140mW dual junction VCSEL diode with diffuser VD-0940V-140M-1C-5AX," May 2022, datasheet, V1. [Online]. Available: https://www.lasercomponents.com/fileadmin/user_upload/home/Datasheets/brightlaser/vd-0940v-140m-1c-bx.pdf
- [75] A.-G. BAuA, "TROS Laserstrahlung - Teil 2: Messungen und Berechnungen von Expositionen gegenüber Laserstrahlung," Jul. 2018.
- [76] M. Dehghani Soltani, H. Kazemi, E. Sarbazi, T. E. H. El-Gorashi, J. M. H. Elmirghani, R. V. Penty, I. H. White, H. Haas, and M. Safari, "High-Speed Imaging Receiver Design for 6G Optical Wireless Communications: A Rate-FOV Trade-Off," *IEEE Trans. Commun.*, vol. 71, no. 2, pp. 1024–1043, Feb. 2023.
- [77] X. Liu, J.-P. M. G. Linnartz, A. M. Khalid, and K. Arulandu, "Response of a Matrix Circuit of Photodiodes with a common Transimpedance Amplifier in Optical Wireless Communications," in *2023 IEEE Wireless Communications and Networking Conference (WCNC)*, Mar. 2023, pp. 1–6.
- [78] T. Koonen and E. Tangdiongga, "Wide Field-of-View Receivers for High-Capacity Optical Wireless Transmission," in *50th European Conference on Optical Communications (ECOC 2024)*, 2024.
- [79] P. Wilke Berenguer, V. Jungnickel, and J. K. Fischer, "The benefit of frequency-selective rate adaptation for optical wireless communications," in *International Symposium on Communication Systems Networks and Digital Signal Processing (CSNDSP)*, IEEE. IEEE, Jul. 2016.
- [80] E. Voges and K. Petermann, Eds., *Optische Kommunikationstechnik: Handbuch für Wissenschaft und Industrie*. Berlin Heidelberg: Springer, 2002.